Interpreting the Dependence of Cloud-Radiative Adjustment on Forcing Agent

Pietro Salvi[1], Paulo Ceppi[1], and Jonathan M. Gregory[2]

[1]Imperial College London
[2]University of Reading

November 21, 2022

Abstract

Effective radiative forcing includes a contribution by rapid adjustments, i.e. changes in temperature, water vapour and clouds that modify the energy budget. Cloud adjustments in particular have been shown to depend strongly on forcing agent. We perform idealised atmospheric heating experiments to demonstrate a relationship between cloud adjustment and the vertical profile of imposed radiative heating: boundary-layer heating causes a positive cloud adjustment, while free-tropospheric heating yields a negative adjustment. This dependence is dominated by the shortwave effect of changes in low clouds. Much of the variation in cloud adjustment among realistic forcing agents such as CO2, CH4, solar forcing, and black carbon is explained by the "characteristic altitude" of the heating profile, through its effect on tropospheric stability.

Interpreting the Dependence of Cloud-Radiative Adjustment on Forcing Agent

Pietro Salvi[1], Paulo Ceppi[1], Jonathan M. Gregory[2,3]

[1]Department of Physics & Grantham Institute, Imperial College London, London, UK
[2]National Centre for Atmospheric Science, University of Reading, Reading, UK
[3]Met Office Hadley Centre, Exeter, UK

Key Points:

- Cloud adjustment depends on the "characteristic altitude" of the atmospheric heating profile
- Boundary-layer (free-tropospheric) heating causes positive (negative) cloud adjustment
- Low clouds dominate the cloud adjustment dependence on forcing altitude

Corresponding author: Pietro Salvi, pietro.salvi14@imperial.ac.uk

Abstract

Effective radiative forcing includes a contribution by rapid adjustments, i.e. changes in temperature, water vapour and clouds that modify the energy budget. Cloud adjustments in particular have been shown to depend strongly on forcing agent. We perform idealised atmospheric heating experiments to demonstrate a relationship between cloud adjustment and the vertical profile of imposed radiative heating: boundary-layer heating causes a positive cloud adjustment, while free-tropospheric heating yields a negative adjustment. This dependence is dominated by the shortwave effect of changes in low clouds. Much of the variation in cloud adjustment among realistic forcing agents such as CO_2, CH_4, solar forcing, and black carbon is explained by the "characteristic altitude" of the heating profile, through its effect on tropospheric stability.

Plain Language Summary

Changes in factors such as greenhouse gas concentrations or solar irradiance affect the balance of energy coming into vs. leaving the earth's atmosphere, a phenomenon known as radiative forcing. This forcing can be modified by rapid atmospheric "adjustments" that occur in temperature, humidity, and cloud cover. The cloud component in particular of these rapid adjustments strongly depends on the forcing agent, for reasons that have been unclear. We find that the vertical structure of atmospheric heating explains much of the forcing agent dependence of the cloud adjustments: bottom-heavier heating causes a more positive cloud adjustment. By understanding what happens when only a small portion of the atmosphere is heated, we show that it is possible to explain cloud adjustments to more complex forcings. We anticipate that our results will provide a physical basis to understand the causes of model-to-model differences in cloud adjustments.

1 Introduction

Radiative forcing quantifies the perturbation to the Earth's energy budget associated with a particular climatic factor, such as greenhouse gases, aerosols or solar irradiance. Forcing was originally defined as the instantaneous perturbation to the Earth's radiative budget due to the forcing agent. Later, the concept was refined to include the effect on the tropospheric heat budget of stratospheric adjustment due to radiative changes, which are particularly important for carbon dioxide (K. Shine et al., 1995). More recently, "effective radiative forcing" (ERF) has become the usual metric (Myhre et al., 2014), which additionally accounts for relatively short-timescale tropospheric adjustments in temperature, moisture and clouds that are direct responses to the forcing, rather than being mediated by surface warming (Andrews & Forster, 2008; Gregory & Webb, 2008; Sherwood et al., 2015). This approach is justified by the fact that ERF is a better predictor of the surface temperature response than instantaneous radiative forcing (IRF) (Richardson et al., 2019) or stratosphere-adjusted forcing (K. P. Shine et al., 2003).

The rapid adjustments to radiative forcing have been found to make a substantial contribution to model uncertainty in ERF for a variety of forcing agents including anthropogenic greenhouse gases, aerosols and solar irradiance (Chung & Soden, 2015; Smith et al., 2018, 2020). Cloud adjustments account for a large part of these differences (Andrews et al., 2012; Colman & McAvaney, 2011; Smith et al., 2018; Zelinka et al., 2013), consistent with clouds being an important source of uncertainty in the response to forcing among climate models (Ceppi et al., 2017), especially in the case of aerosols. Aerosol–*radiation* interactions lead to cloud adjustments (known as semi-direct effects) by modifying local atmospheric conditions. Aerosol–*cloud* interactions lead to further cloud adjustments via microphysical changes (known as indirect effects; Bellouin et al., 2020). Only the cloud adjustments due to semi-direct effects will be considered in this paper.

Several past papers have investigated the mechanisms of cloud adjustments in response to CO_2 forcing (e.g., Dinh & Fueglistaler, 2017; Kamae & Watanabe, 2012, 2013; Kamae et al., 2015, 2019; Zelinka et al., 2013) and to absorbing aerosols such as black carbon (BC) (Ban-Weiss et al., 2012; Bellouin et al., 2020; Koch & Del Genio, 2010; Samset & Myhre, 2015; Stjern et al., 2020) or dust (Amiri-Farahani et al., 2017), but there is a lack of process studies involving other forcing agents. Smith et al. (2018) demonstrated a striking forcing agent dependence of cloud adjustments across Coupled Model Intercomparison Project phase 5 (CMIP5) models, with consistently positive adjustments to CO_2 and negative adjustments to solar and BC forcing. However, there is currently limited understanding of how different cloud adjustments arise in response to various instantaneous forcings.

In this study we address this knowledge gap by interpreting the forcing agent dependence of cloud adjustment in terms of the spatial structure of instantaneous atmospheric forcing. Specifically, we propose here that the vertical profile of atmospheric heating is a key factor for this forcing agent dependence. For absorbing aerosols, previous studies have identified a dependence of semi-direct cloud adjustments upon forcing altitude: typically positive for boundary-layer forcing, negative for free-tropospheric forcing (Amiri-Farahani et al., 2017; Ban-Weiss et al., 2012; Bellouin et al., 2020; Koch & Del Genio, 2010; Samset & Myhre, 2015; Stjern et al., 2020). Here we show that this dependence on the vertical heating profile also accounts for much of the cloud adjustment dependence on diverse forcing agents. This is demonstrated through comparison of idealised and realistic forcing experiments with a CMIP5-class climate model.

2 Data and Methods

The simulations used for this paper were run with the CAM4 model (Neale et al., 2010) in an atmosphere-only configuration with prescribed sea surface temperatures (SSTs) and sea ice concentrations. A $1.9^{\circ}\times 2.5^{\circ}$ latitude/longitude grid was used with 26 vertical levels. Simulations were run for 20 years with the climatology calculated as the average of monthly-mean data output from the model for all but the first simulated year, during which the atmosphere was adjusting to reach a steady state in the presence of the forcing. The vertical profiles shown in this paper were linearly interpolated from the model's 26 hybrid sigma–pressure levels to a finer 100-level pressure grid, with evenly spaced levels between 0 and 1000 hPa.

Instantaneous and effective radiative forcings were calculated for four forcing agents, listed in Table S1. These are among the same forcing agents as in the Precipitation Driver Response Model Intercomparison Project (PDRMIP) set of experiments (Myhre et al., 2017), although not all with the same concentrations. IRF was calculated using the Parallel Offline Radiative Transfer (PORT) tool for CAM4 (Conley et al., 2013). To obtain ERF, the difference in mean climate was taken between perturbed and control CAM4 experiments with SSTs and sea ice fixed to the control state (Hansen et al., 1997). Note that the CO_2 concentration was doubled only in the radiation scheme in the $2\times CO_2$ experiment, so the model did not simulate a plant physiological response to CO_2, which has been found to cause significant cloud-radiative adjustments (Doutriaux-Boucher et al., 2009). Furthermore, CAM4 does not simulate aerosol–cloud interactions for black carbon, whose atmospheric concentrations are prescribed.

In addition to the realistic forcing cases (Table S1), experiments were also performed with idealised, horizontally homogeneous forcings (Table S2), prescribed as an extra heating rate in CAM4's radiation scheme. This includes uniform 4 W m^{-2} atmospheric (atm_4) and surface (sfc_4) forcing, as well as vertically-localised forcings at specific atmospheric levels ϕ (vloc_ϕhPa; Fig. S1). The applied heating rate anomalies for the vloc_ϕhPa forcing experiments were defined as follows:

$$\begin{aligned} \Delta Q(p) = &\quad A\cos^2\left(\frac{(p-\phi)\pi}{2a}\right) &&\text{for } (\phi-a) \le p \le (\phi+a) \\ \Delta Q(p) = &\quad 0 &&\text{otherwise} \end{aligned} \tag{1}$$

for pressure p and heating centred at ϕ, where $A = \pm 0.135$ K day^{-1}, $a = 125$ hPa, and ΔQ is the instantaneous atmospheric heating anomaly from the control. This provides a vertically-integrated forcing of 2 W m^{-2}, except for the topmost and lowermost vertically-localised experiments which are truncated at the pressure limits (Fig. S1) and thus provide around half the vertically-integrated forcing. The whole atmosphere was covered by nine of these bounded $\cos^2$ heating profiles centred on multiples of 125 hPa between 0 and 1000 hPa (inclusive). The $\cos^2$ shape combined with the $2a$ heating profile widths mean that the sum of these profiles is uniform in pressure. The width a was chosen such that the forcings are sufficiently localised in the vertical, while still being adequately resolved by CAM4's vertical grid. To test the linearity of the responses, both positive and negative vertically localised forcings were applied.

Rather than calculating cloud adjustments as differences in cloud-radiative effect (CRE), we use cloud kernels from Zelinka et al. (2012) (see Fig. S2). Unlike CRE differences, which are affected by non-cloud adjustments (in temperature, water vapour or surface albedo), the kernels quantify the radiative impact of cloud adjustment in isolation. A further benefit to using cloud kernels is that the radiative adjustments can be broken down by cloud top pressure (CTP) into contributions from high (CTP $<$ 440 hPa), mid (440 $<$ CTP $<$ 680 hPa), and low (CTP $>$ 680 hPa) clouds. To use the cloud kernels, the International Satellite Cloud Climatology Project (ISCCP) satellite simulator (Swales et al., 2018) was enabled in CAM4 to output the required cloud fraction histograms (see Fig. S2 for an example).

We introduce two measures in this paper to help understand the relationship between the vertical profile of atmospheric forcing, tropospheric stability, and cloud-radiative adjustment. Firstly, to characterise the vertical distribution of forcing $Q(p)$ we define a "heating-weighted pressure centroid":

$$\frac{\int_{p=200\,\mathrm{hPa}}^{1000\,\mathrm{hPa}} p \cdot Q(p)\, dp}{\int_{p=200\,\mathrm{hPa}}^{1000\,\mathrm{hPa}} Q(p)\, dp} \tag{2}$$

This is understood as the "centre of mass" of the forcing, defined such that larger values here denote a bottom-heavier atmospheric forcing profile. Note that the pressure centroid is positive for the vertically-localised heatings of either sign. In general, the pressure centroid is positive and readily interpreted for atmospheric forcings which are entirely or mostly of the same sign at all pressures, as is the case for all those we consider.

Secondly, for tropospheric stability we define the "bulk tropospheric stability" (BTS) as the difference between the average potential temperature (Θ) for the 200–800 hPa layer ($\Theta_{200-800}$), taken as representative of the free troposphere, and $\Theta_{800-1000}$, taken as representative of the boundary layer:

$$\mathrm{BTS} = \Theta_{200-800} - \Theta_{800-1000}. \tag{3}$$

3 Vertically Localised Atmospheric Heating Experiments

To gain insight into the dependence of cloud adjustments on forcing altitude, we begin with the results from the vertically-localised forcing experiments. Focusing on the vertical structure, Fig. 1 shows the global-mean adjustments of temperature (T), relative humidity (RH) and cloud fraction for three of the vertically-localised forcings (chosen as examples). A close correspondence is found between the peak of applied heating

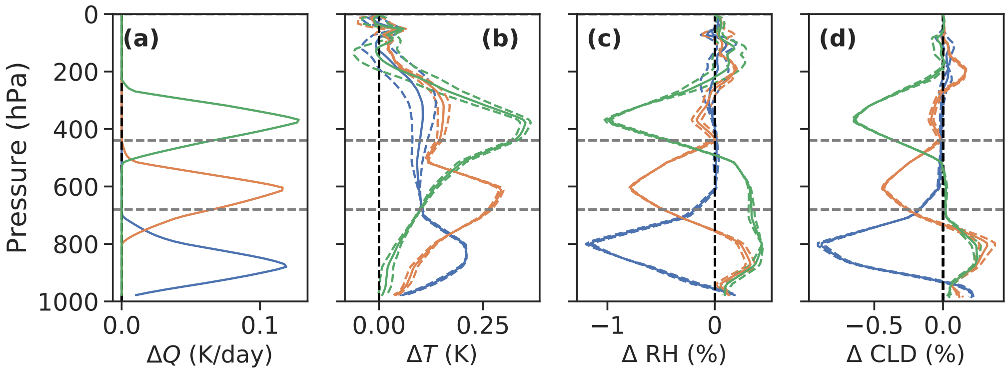

Figure 1. Profiles for (a) applied heating rates ΔQ, as well as (b) temperature, (c) relative humidity, and (d) cloud fraction (CLD) change profiles for vertically-localised heating experiments with $\phi = 875$ hPa (*blue*), $\phi = 625$ hPa (*orange*), and $\phi = 375$ hPa (*green*). Profiles shown in solid lines are the average of the positive (heating) and negative of the negative (cooling) vertically-localised forcings set at the same heights and magnitudes, with these shown separately with dashed lines. Heating profiles are interpolated from model input, rather than those defined in Eq. 1. The grey horizontal lines demarcate bounds between high, mid, and low levels according to the ISCCP simulator. Changes to temperature, relative humidity, and cloud are obtained as the difference between the equilibrium fixed SST state and a control state.

and the peaks of changes to T and RH, as well as cloud fraction. Furthermore, there is a striking similarity between the profiles of changes to RH and cloud fraction, as expected.

In addition to the expected local responses, the vertically-localised forcings also cause non-local changes via changes in stratification and their impacts on vertical heat and moisture fluxes. Heating at lower levels (in the boundary layer) destabilises the overlying free troposphere, leading to enhanced convection and vertical mixing and resulting in warming at higher levels, but little change in RH or cloud (Fig. 1, blue curves). By contrast, free-tropospheric heating causes suppressed convection at lower levels through increased tropospheric stability (Fig. 2a, open symbols indicate greater positive ΔBTS for vertically-localised heatings at lower pressure, which means higher altitude), leading to increases to RH and cloud fraction at lower levels (Fig. 1, orange and green curves).

In summary, cloud fraction decreases in response to localised heating at all levels and associated drying, but low-level cloud increases in response to heating at higher levels. The latter is consistent with the known dependence of low clouds on tropospheric stability (Klein & Hartmann, 1993). Generally, these results are consistent with those from Samset and Myhre (2015, their Fig. 5) involving application of localised BC layers at different atmospheric levels.

Differences between the responses to vertically-localised heating and cooling are minor (dashed lines in Fig. 1), and are mainly noticeable for the temperature response. Differences in cloud-radiative adjustments between vertically-localised positive and negative heating are also minor (see discussion below).

There is a strong dependence of the cloud-radiative adjustments on the altitude of applied forcing and the associated stability changes. The net cloud adjustments in Fig. 2d are of substantial magnitude relative to the imposed vertically-localised forcings of 2 W m^{-2} – ranging from about -50% to $+20\%$ of the imposed forcing. This illustrates how

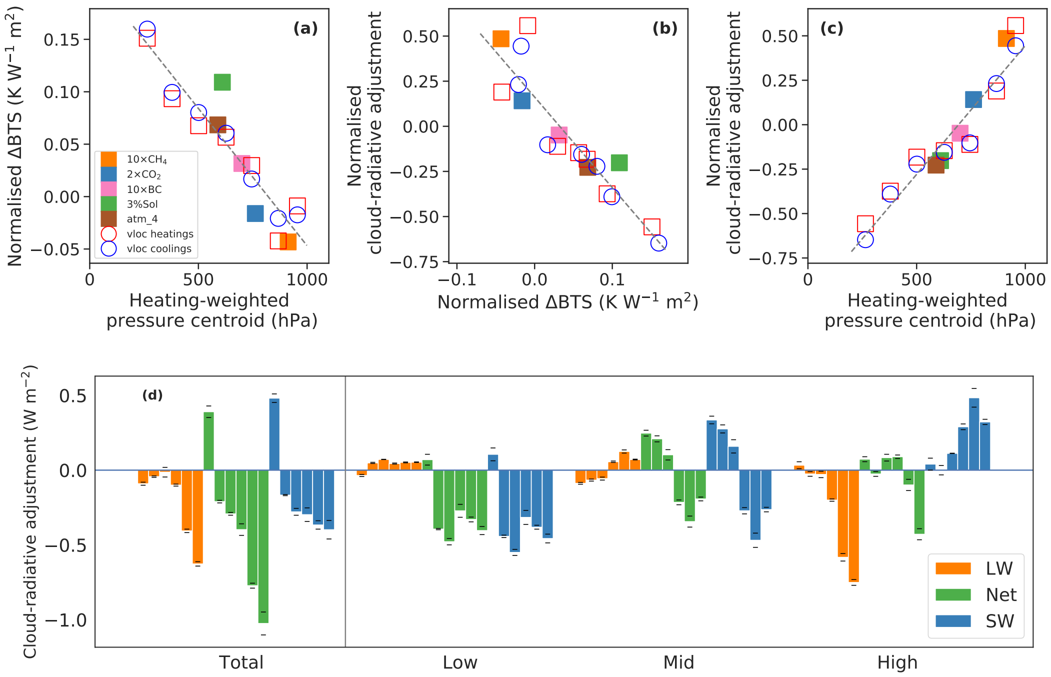

Figure 2. (a) Changes to bulk tropospheric stability (BTS, see Eq. 3), normalised by the the vertically-integrated tropospheric (200–1000 hPa) forcings, versus the vertical centre of mass of tropospheric heating (Eq. 2) for each experiment performed in this study. (b) Normalised cloud-radiative adjustments against normalised BTS changes. (c) Normalised cloud-radiative adjustments versus heating centre of mass. Least-squares linear fits are shown by the dashed lines. Only experiments with significant tropospheric forcing are shown, which excludes the 0 hPa and 125 hPa forcing experiments. (d) Cloud-radiative adjustments from the six vertically-localised forcings centered between 875 and 250 hPa, in 125-hPa increments, with increasing altitude of applied heating from left to right within each coloured grouping. The lowest altitude forcing at 1000 hPa is excluded because it is truncated; furthermore, the two highest altitude forcings are excluded because they are mainly in the stratosphere, and have little impact on clouds. Individual bars represent the averages between the responses to heatings and the negative of the responses to coolings at the same altitudes and of the same magnitudes, with the thin horizontal lines around the bars representing the results from those individual experiments.

cloud adjustments can substantially enhance or offset the instantaneous forcing, depending on the vertical distribution of heating. (Note that for the vertically localised cases the IRF equals the atmospheric heating, since there is no surface forcing, unlike in more realistic cases.) The cloud-radiative adjustment is increasingly negative with increasing height of the applied localised heating (Fig. 2c–d). This is driven by both LW and SW changes, with the latter dominating, qualitatively consistent with previous findings for BC forcing applied at different altitudes (Samset & Myhre, 2015, their Fig. 1). SW cloud adjustments flip sign from positive to negative as forcing altitude increases, while LW cloud adjustments become strongly negative (Fig. 2d). The dependence of LW cloud adjustment on forcing altitude is consistent with the understanding that LW cloud-radiative effect increases with cloud altitude (Hartmann, 1994), due to increased temperature differences between higher clouds and the surface.

To interpret the dependence of SW cloud adjustment on forcing altitude, it is helpful to consider the breakdown of the adjustments into contributions by high-, mid- and low-level clouds in Fig. 2d. The contributions are positive at the level of the heating, but negative below. This is consistent with the findings from Fig. 1: localised heating causes a cloud fraction reduction locally, but a cloud fraction increase below (particularly in the boundary layer), associated with stabilisation (Fig. 2, open symbols) and suppressed vertical mixing. There is an additional factor contributing to the negative SW cloud adjustment below the vertically-localised heating: when cloud fraction decreases at the heating level, the reduced overlap reveals and hence increases SW reflection from lower-level clouds.

In addition to the effect of atmospheric forcing, cloud adjustments could also result from surface-mediated heating. However, we find that the effect of surface forcing is very small: the net cloud-radiative adjustment for the sfc_4 case is -0.03 W m^{-2}, with similarly small adjustment contributions across cloud altitudes and in the LW and SW. This is negligible in comparison to the adjustments for the localised atmospheric heating experiments, especially per unit of forcing. This result is expected given the fixed-SST lower boundary, where surface forcing can impact the atmosphere only over land and ice regions. Note that although the rapid climate response to land warming under fixed SSTs is typically included in the ERF as part of the rapid adjustment (Forster et al., 2016; Sherwood et al., 2015), conceptually this can also be treated as a surface warming–driven radiative response (Chung & Soden, 2015; K. P. Shine et al., 2003).

4 Interpreting Cloud-Radiative Adjustments to Realistic Forcing Agents

Having established how cloud adjustments depend on the vertical profile of atmospheric heating in section 3, this section investigates what this information provides in understanding cloud adjustments to vertically-distributed atmospheric forcings, mainly through trying to understand adjustments to realistic forcing agents (Table S1). For each of the realistic forcings (as well as the idealised atm_4 case) we express the vertical profile of global-mean IRF as a linear combination of idealised vertically-localised heatings:

$$\Delta Q_{\mathrm{fit}}(p) = \sum_{i=1}^{9} \left(a_i \cdot \Delta Q_i(p) \right), \tag{4}$$

where ΔQ_i and a_i are the anomalous heating rates (i.e. the IRF) and fitting coefficients respectively for each of the nine vertically-localised forcings i. The a_i coefficients were calculated so as to minimise the least-squares difference between Q_{fit} and the global-mean heating profile of a chosen case, Q_{case} (Fig. 3, left column). Best-fits are expected to be unique given that the profiles of the vertically-localised forcings are mostly non-overlapping and hence mostly orthogonal.

The heating profiles for the realistic forcings (and atm_4) are very closely approximated by linearly combining the nine idealised vertically-localised cases (Fig. 3, left column). The only deviations occur above the tropopause for the $2\times CO_2$ and 3%Sol cases where there is insufficient vertical resolution in the localised forcing experiments.

We then estimate the globally-averaged vertical profiles of change in temperature, relative humidity, and cloud fraction (each denoted by X) in response to vertically-distributed forcings thus:

$$\Delta X_{\mathrm{fit}}(p) = \left(\frac{F_{\mathrm{case,sfc}}}{4} \cdot \Delta X_{\mathrm{sfc\_4}} \right) + \sum_i \left(a_i \cdot \Delta X_i(p) \right). \qquad (5)$$

The first term on the right-hand side accounts for contributions from surface forcing, using the results from a 4 W m^{-2} uniform surface forcing experiment (sfc_4, see Table S2), appropriately weighted for the surface forcing $F_{\mathrm{case,sfc}}$ of the reference case. (Although surface forcing causes a very small adjustment per unit forcing, we found the surface contribution to be non-negligible for the 3%Sol experiment – see below.)

The linear combination of idealised vertically-localised heatings closely approximates the adjustments of temperature, RH and cloud fraction diagnosed from the model (Fig. 3). This suggests that the global-average vertical structure of these adjustments is primarily determined by the vertical profile of IRF.

The contributions to these profiles from the surface components of the forcings were found to be minor in general, consistent with our finding that the cloud adjustment to uniform surface-only forcing is very small. The notable exception to this was in the solar forcing case, where the majority of instantaneous forcing is from the surface component (4.88 W m^{-2}, compared to a 2.19 W m^{-2} atmospheric component), such that the surface component makes a non-negligible contribution to the cloud fraction change profile (Fig. S4).

Considering the global average top-of-atmosphere cloud-radiative adjustments to forcings, we find that the linear combinations of vertically-localised heating experiments generally predict the correct sign, and to a lesser extent magnitude, of the vertically-distributed forcings (Fig. 4). The largest errors are for CO_2 and CH_4, where the positive SW adjustments are considerably underestimated. Inspection of the cloud fraction profiles in Fig. 3 suggests this may partly result from an underestimation of the lower-tropospheric cloud fraction decrease by the simple linear combination method, and potentially from differences in estimation of cloud changes near the tropopause. That the predicted net adjustments are more accurate than the individual SW and LW adjustments can be explained by compensating errors in SW and LW. Errors in this approach may also result from the linear combination of cloud-radiative adjustments being unable to account for the non-linear effects of cloud overlap.

Nevertheless, the results in Figs. 3 and 4 account for the finding of Fig. 2c (filled symbols) that the sign and magnitude of cloud-radiative adjustments are mostly explained by the vertical structure of the instantaneous atmospheric forcing, as measured by the heating-weighted pressure centroid. Positive CRE adjustments result from the "bottom-heaviest" IRFs $2\times CO_2$ and $10\times CH_4$, negative CRE adjustments from 3%Sol and atm_4, whose IRFs are fairly uniform with altitude, while 10xBC is intermediate.

Although our interpretation is based on a single climate model, we note that the cloud-radiative adjustments in Fig. 4 are reasonably representative of those simulated by a range of CMIP5 models (Fig. 4 of Smith et al., 2018). In particular, models consistently simulate positive cloud-radiative adjustments to CO_2, and negative adjustments to solar forcing, in agreement with our results. Note that the results of Smith et al. (2018) use different magnitudes of the CH_4 and solar forcings, and include the stomatal conductance effect of $2\times CO_2$. Increases to CO_2 lead to reduced to evapotranspiration and thus reduced low cloud over many highly forested areas for a positive effect on the cloud-radiative adjustment (Doutriaux-Boucher et al., 2009). We found that including this ef-

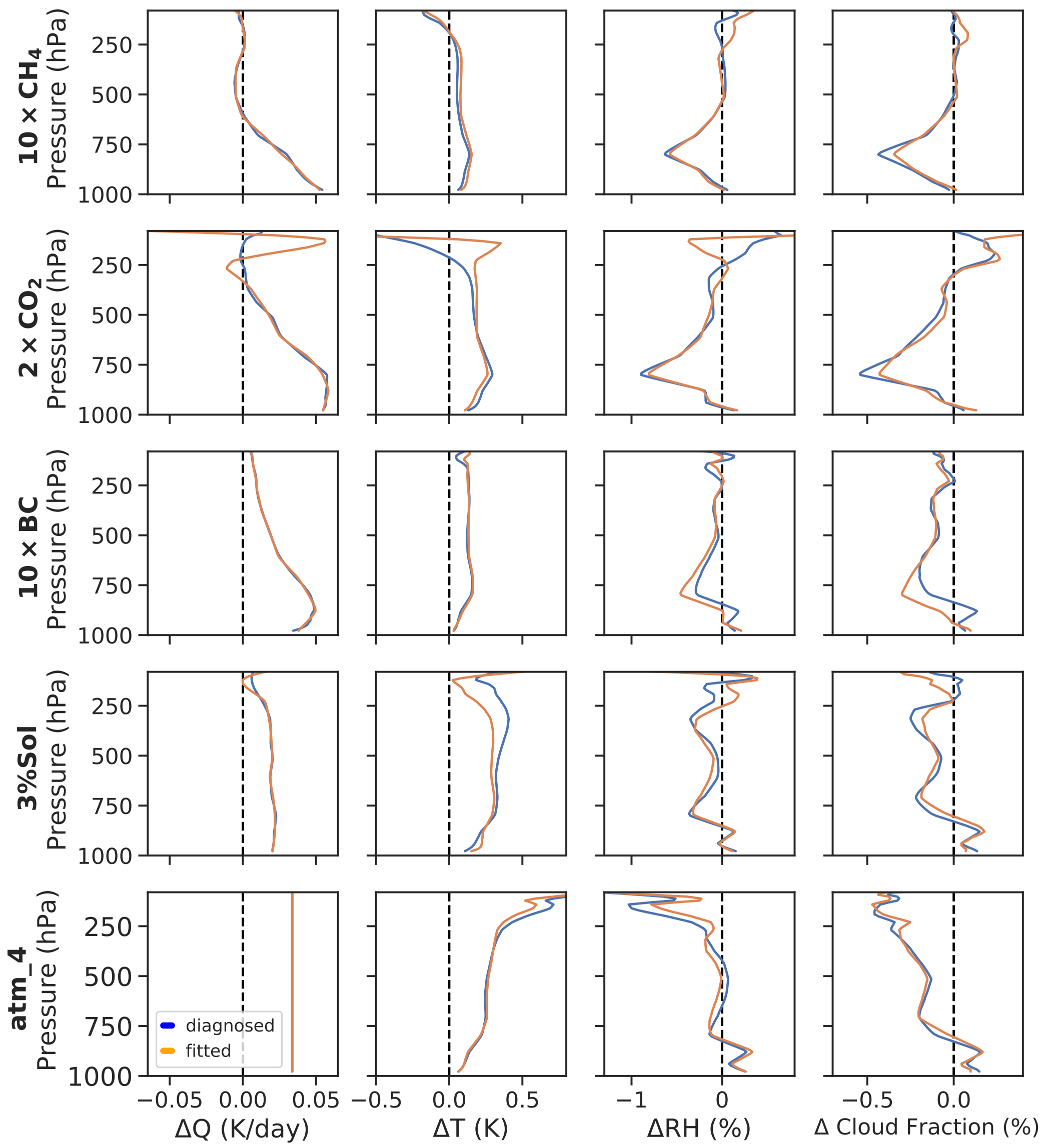

Figure 3. Global-mean vertical profiles of IRF (ΔQ) and rapid adjustments of temperature (ΔT), relative humidity ($\Delta \mathrm{RH}$) and cloud fraction. Shown are the results from the original cases (*blue*) and linear combinations of the results from the vertically-localised forcing experiments (*orange*) including an appropriate surface term (Eq. 5). Fitted heating rates are best fits to the original heating rates (Eq. 4), whilst the orange lines for other variables are created from the fits of heating rates (Eq. 5).

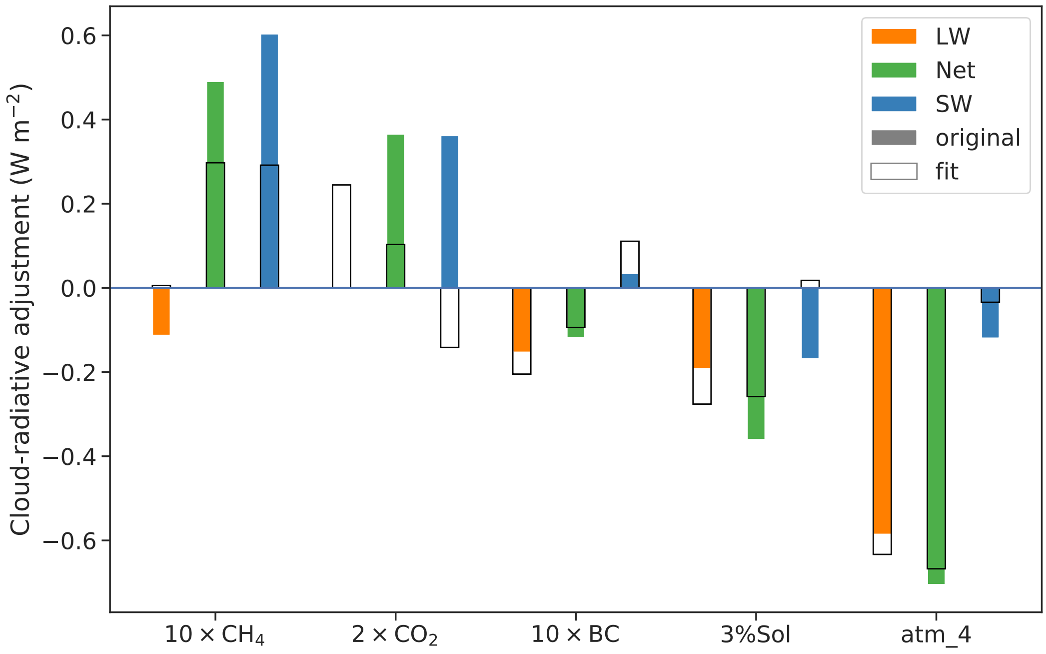

Figure 4. A comparison of the cloud-radiative adjustments predicted from linearly combining vertically-localised forcing experiments (*hatched bars*) versus the radiative adjustments calculated from the relevant experiments themselves (*solid bars*).

fect approximately doubles the cloud adjustment to 2×CO_2 forcing in CAM4 (0.76 vs 0.37 W m^{-2}; not shown).

5 Summary and Conclusions

We have demonstrated through a series of idealised experiments with vertically-localised atmospheric heating that cloud-radiative adjustments are sensitive principally to the altitude of atmospheric heating caused instantaneously by the forcing agent. At levels where there is instantaneous positive heating, the air becomes warmer and drier and the cloud fraction decreases. However, positive heating at any level above the boundary layer stabilises the troposphere below and suppresses vertical mixing, thus causing moistening and increased cloud fraction at lower levels. As the net result of these two effects, lower-tropospheric heating results in positive cloud-radiative adjustment (dominated by the SW effect of reduced low cloud fraction), while mid- and upper-tropospheric heating causes negative adjustment (due to the combined LW and SW effects of increased low cloud and reduced free-tropospheric cloud). For negative forcings, the signs of all effects are reversed and the magnitudes are similar.

We find that the global-mean cloud-radiative adjustments to realistic forcings can be reasonably well explained by linearly combining the idealised vertically-localised forcings so as to fit the vertical heating profiles caused by the various forcing agents. In particular, our results suggest that positive cloud adjustment commonly found in GCMs to the greenhouse gas forcing agents CO_2 and CH_4 is explained by their relatively bottom-heavy profiles of instantaneous radiative forcing; by contrast, the negative cloud adjustment to solar forcing is caused by its relatively larger free-tropospheric heating. Our findings are consistent also with previous evidence that cloud-radiative adjustments depend on the altitude of absorbing aerosols such as black carbon (Samset & Myhre, 2015; Allen et al., 2019).

Although successful in explaining the sign and relative magnitude of adjustments for different agents, our method using global-mean vertical profiles does not give quantitatively accurate estimates. This may be for instance because of neglecting the geographical pattern and the seasonal cycle of the instantaneous heating, perhaps especially the contrast between its effects in cloudy and cloud-free air. Further investigation is needed of these aspects. With such refinement, we expect that this approach will provide a useful basis to interpret inter-model differences in cloud adjustments, to the extent that such differences result from uncertainties in the distribution of instantaneous radiative forcing.

Acknowledgments

PS was supported by the Department of Physics and the Grantham Institute of Imperial College London. PC was supported by an Imperial College Research Fellowship and NERC grants NE/T006250/1 and NE/T007788/1. JMG was supported by the European Research Council under the European Union's Horizon 2020 research and innovation programme (grant agreement No 786427, project "Couplet"). This work used JASMIN, the UK collaborative data analysis facility and the ARCHER UK National Supercomputing Service.

The data that support the findings of this study are available from `https://doi.org/10.6084/m9.figshare.14386799`

References

Allen, R. J., Amiri-Farahani, A., Lamarque, J.-F., Smith, C., Shindell, D., Hassan, T., & Chung, C. E. (2019, December). Observationally constrained aerosol–cloud semi-direct effects. *npj Climate and Atmospheric Science*, *2*(1), 16. Retrieved 2020-02-04, from `http://www.nature.com/articles/s41612-019-0073-9` doi: 10.1038/s41612-019-0073-9

Amiri-Farahani, A., Allen, R. J., Neubauer, D., & Lohmann, U. (2017, May). Impact of Saharan dust on North Atlantic marine stratocumulus clouds: importance of the semidirect effect. *Atmospheric Chemistry and Physics*, *17*(10), 6305–6322. Retrieved 2021-01-25, from `https://acp.copernicus.org/articles/17/6305/2017/` (Publisher: Copernicus GmbH) doi: https://doi.org/10.5194/acp-17-6305-2017

Andrews, T., & Forster, P. M. (2008). CO2 forcing induces semi-direct effects with consequences for climate feedback interpretations. *Geophysical Research Letters*, *35*(4). Retrieved 2021-01-12, from `https://agupubs.onlinelibrary.wiley.com/doi/abs/10.1029/2007GL032273` (_eprint: https://agupubs.onlinelibrary.wiley.com/doi/pdf/10.1029/2007GL032273) doi: https://doi.org/10.1029/2007GL032273

Andrews, T., Gregory, J. M., Forster, P. M., & Webb, M. J. (2012, July). Cloud Adjustment and its Role in CO2 Radiative Forcing and Climate Sensitivity: A Review. *Surveys in Geophysics*, *33*(3), 619–635. Retrieved 2019-07-15, from `https://doi.org/10.1007/s10712-011-9152-0` doi: 10.1007/s10712-011-9152-0

Ban-Weiss, G. A., Cao, L., Bala, G., & Caldeira, K. (2012, March). Dependence of climate forcing and response on the altitude of black carbon aerosols. *Climate Dynamics*, *38*(5), 897–911. Retrieved 2020-10-21, from `https://doi.org/10.1007/s00382-011-1052-y` doi: 10.1007/s00382-011-1052-y

Bellouin, N., Quaas, J., Gryspeerdt, E., Kinne, S., Stier, P., Watson-Parris, D., ... Stevens, B. (2020). Bounding Global Aerosol Radiative Forcing of Climate Change. *Reviews of Geophysics*, *58*(1), e2019RG000660. Retrieved 2021-02-01, from https://agupubs.onlinelibrary.wiley.com/doi/abs/10.1029/2019RG000660 (_eprint: https://agupubs.onlinelibrary.wiley.com/doi/pdf/10.1029/2019RG000660) doi: https://doi.org/10.1029/2019RG000660

Ceppi, P., Brient, F., Zelinka, M. D., & Hartmann, D. L. (2017). Cloud feedback mechanisms and their representation in global climate models. *Wiley Interdisciplinary Reviews: Climate Change*, *8*(4), e465. Retrieved 2019-07-15, from https://onlinelibrary.wiley.com/doi/abs/10.1002/wcc.465 doi: 10.1002/wcc.465

Chung, E.-S., & Soden, B. J. (2015, March). An Assessment of Direct Radiative Forcing, Radiative Adjustments, and Radiative Feedbacks in Coupled Ocean–Atmosphere Models. *Journal of Climate*, *28*(10), 4152–4170. Retrieved 2019-07-15, from https://journals.ametsoc.org/doi/full/10.1175/JCLI-D-14-00436.1 doi: 10.1175/JCLI-D-14-00436.1

Colman, R. A., & McAvaney, B. J. (2011, April). On tropospheric adjustment to forcing and climate feedbacks. *Climate Dynamics*, *36*(9), 1649. Retrieved 2019-09-20, from https://doi.org/10.1007/s00382-011-1067-4 doi: 10.1007/s00382-011-1067-4

Conley, A. J., Lamarque, J.-F., Vitt, F., Collins, W. D., & Kiehl, J. (2013, April). PORT, a CESM tool for the diagnosis of radiative forcing. *Geoscientific Model Development*, *6*(2), 469–476. Retrieved 2019-07-15, from https://www.geosci-model-dev.net/6/469/2013/ doi: https://doi.org/10.5194/gmd-6-469-2013

Dinh, T., & Fueglistaler, S. (2017). Mechanism of Fast Atmospheric Energetic Equilibration Following Radiative Forcing by CO2. *Journal of Advances in Modeling Earth Systems*, *9*(7), 2468–2482. Retrieved 2019-07-15, from https://agupubs.onlinelibrary.wiley.com/doi/abs/10.1002/2017MS001116 doi: 10.1002/2017MS001116

Doutriaux-Boucher, M., Webb, M. J., Gregory, J. M., & Boucher, O. (2009). Carbon dioxide induced stomatal closure increases radiative forcing via a rapid reduction in low cloud. *Geophysical Research Letters*, *36*(2). Retrieved 2019-09-20, from https://agupubs.onlinelibrary.wiley.com/doi/abs/10.1029/2008GL036273 doi: 10.1029/2008GL036273

Forster, P. M., Richardson, T., Maycock, A. C., Smith, C. J., Samset, B. H., Myhre, G., … Schulz, M. (2016). Recommendations for diagnosing effective radiative forcing from climate models for CMIP6. *Journal of Geophysical Research: Atmospheres*, *121*(20), 12,460–12,475. Retrieved 2020-01-21, from https://agupubs.onlinelibrary.wiley.com/doi/abs/10.1002/2016JD025320 doi: 10.1002/2016JD025320

Gregory, J., & Webb, M. (2008, January). Tropospheric Adjustment Induces a Cloud Component in CO2 Forcing. *Journal of Climate*, *21*(1), 58–71. Retrieved 2019-07-15, from https://journals.ametsoc.org/doi/full/10.1175/2007JCLI1834.1 doi: 10.1175/2007JCLI1834.1

Hansen, J., Sato, M., & Ruedy, R. (1997). Radiative forcing and climate response. *Journal of Geophysical Research: Atmospheres*, *102*(D6), 6831–6864. Retrieved 2019-08-09, from https://agupubs.onlinelibrary.wiley.com/doi/abs/10.1029/96JD03436 doi: 10.1029/96JD03436

Hartmann, D. L. (1994). *Global physical climatology*. San Diego ; London: Academic Press.

Kamae, Y., Chadwick, R., Ackerley, D., Ringer, M., & Ogura, T. (2019, May). Seasonally variant low cloud adjustment over cool oceans. *Climate Dynamics*, *52*(9-10), 5801–5817. Retrieved 2019-09-16, from http://link.springer.com/10.1007/s00382-018-4478-7 doi: 10.1007/s00382-018-4478-7

Kamae, Y., & Watanabe, M. (2012). On the robustness of tropospheric adjustment in CMIP5 models. *Geophysical Research Let-*

ters, *39*(23). Retrieved 2020-04-28, from https://agupubs.onlinelibrary.wiley.com/doi/abs/10.1029/2012GL054275 (_eprint: https://agupubs.onlinelibrary.wiley.com/doi/pdf/10.1029/2012GL054275) doi: 10.1029/2012GL054275

Kamae, Y., & Watanabe, M. (2013, December). Tropospheric adjustment to increasing CO2: its timescale and the role of land–sea contrast. *Climate Dynamics*, *41*(11-12), 3007–3024. Retrieved 2019-07-04, from http://link.springer.com/10.1007/s00382-012-1555-1 doi: 10.1007/s00382-012-1555-1

Kamae, Y., Watanabe, M., Ogura, T., Yoshimori, M., & Shiogama, H. (2015, June). Rapid Adjustments of Cloud and Hydrological Cycle to Increasing CO2: a Review. *Current Climate Change Reports*, *1*(2), 103–113. Retrieved 2019-07-04, from http://link.springer.com/10.1007/s40641-015-0007-5 doi: 10.1007/s40641-015-0007-5

Klein, S. A., & Hartmann, D. L. (1993, August). The Seasonal Cycle of Low Stratiform Clouds. *Journal of Climate*, *6*(8), 1587–1606. Retrieved 2020-12-18, from https://journals.ametsoc.org/view/journals/clim/6/8/1520-0442_1993_006_1587_tscols_2_0_co_2.xml (Publisher: American Meteorological Society Section: Journal of Climate) doi: 10.1175/1520-0442(1993)006⟨1587:TSCOLS⟩2.0.CO;2

Koch, D., & Del Genio, A. D. (2010, August). Black carbon semi-direct effects on cloud cover: review and synthesis. *Atmospheric Chemistry and Physics*, *10*(16), 7685–7696. Retrieved 2021-01-25, from https://acp.copernicus.org/articles/10/7685/2010/ doi: 10.5194/acp-10-7685-2010

Myhre, G., Forster, P. M., Samset, B. H., Hodnebrog, O., Sillmann, J., Aalbergsjø, S. G., … Zwiers, F. (2017, June). PDRMIP A Precipitation Driver and Response Model Intercomparison Project—Protocol and Preliminary Results. *Bulletin of the American Meteorological Society*, *98*(6), 1185–1198. Retrieved 2019-08-01, from http://journals.ametsoc.org/doi/10.1175/BAMS-D-16-0019.1 doi: 10.1175/BAMS-D-16-0019.1

Myhre, G., Shindell, D., Bréon, F.-M., Collins, W., Fuglestvedt, J., Huang, J., … Zhang, H. (2014). *Anthropogenic and Natural Radiative Forcing. In: Climate Change 2013: The Physical Science Basis. Contribution of Working Group I to the Fifth Assessment Report of the Intergovernmental Panel on Climate Change* (Tech. Rep. No. AR5). Retrieved from https://www.ipcc.ch/report/ar5/wg1/ (Publisher: Cambridge University Press)

Neale, R. B., Richter, J. H., Conley, A. J., Park, S., Lauritzen, P. H., Gettelman, A., … Lin, S.-J. (2010, April). *Description of the NCAR Community Atmosphere Model (CAM 4.0).*

Richardson, T. B., Forster, P. M., Smith, C. J., Maycock, A. C., Wood, T., Andrews, T., … Watson-Parris, D. (2019). Efficacy of Climate Forcings in PDRMIP Models. *Journal of Geophysical Research: Atmospheres*, *124*(23), 12824–12844. Retrieved 2020-01-17, from https://agupubs.onlinelibrary.wiley.com/doi/abs/10.1029/2019JD030581 doi: 10.1029/2019JD030581

Samset, B. H., & Myhre, G. (2015). Climate response to externally mixed black carbon as a function of altitude. *Journal of Geophysical Research: Atmospheres*, *120*(7), 2913–2927. Retrieved 2019-10-04, from https://agupubs.onlinelibrary.wiley.com/doi/abs/10.1002/2014JD022849 doi: 10.1002/2014JD022849

Sherwood, S. C., Bony, S., Boucher, O., Bretherton, C., Forster, P. M., Gregory, J. M., & Stevens, B. (2015, February). Adjustments in the Forcing-Feedback Framework for Understanding Climate Change. *Bulletin of the American Meteorological Society*, *96*(2), 217–228. Retrieved 2020-12-10, from https://journals.ametsoc.org/view/journals/bams/96/2/bams-d-13-00167.1.xml (Publisher: American Meteorological Society Section: Bulletin of the American

Meteorological Society) doi: 10.1175/BAMS-D-13-00167.1

Shine, K., Fouquart, Y., Ramaswamy, V., Solomon, S., & Srinivasan, J. (1995). *Radiative Forcing. In: IPCC Report on Radiative Forcing of Climate Change and An Evaluation of the IPCC IS92 Emission Scenarios* (Tech. Rep.). Retrieved 2021-01-14, from `https://www.ipcc.ch/report/climate-change-1994-radiative-forcing-of-climate-change-and-an-evaluation-of-the-ipcc-is92-emission-scenarios-2/`

Shine, K. P., Cook, J., Highwood, E. J., & Joshi, M. M. (2003). An alternative to radiative forcing for estimating the relative importance of climate change mechanisms. *Geophysical Research Letters*, *30*(20). Retrieved 2021-01-11, from `https://agupubs.onlinelibrary.wiley.com/doi/abs/10.1029/2003GL018141` (_eprint: https://agupubs.onlinelibrary.wiley.com/doi/pdf/10.1029/2003GL018141) doi: https://doi.org/10.1029/2003GL018141

Smith, C. J., Kramer, R. J., Myhre, G., Alterskjær, K., Collins, W., Sima, A., … Forster, P. M. (2020, January). *Effective radiative forcing and adjustments in CMIP6 models* (preprint). Radiation/Atmospheric Modelling/Troposphere/Physics (physical properties and processes). Retrieved 2020-02-05, from `https://www.atmos-chem-phys-discuss.net/acp-2019-1212/` doi: 10.5194/acp-2019-1212

Smith, C. J., Kramer, R. J., Myhre, G., Forster, P. M., Soden, B. J., Andrews, T., … Watson-Parris, D. (2018). Understanding Rapid Adjustments to Diverse Forcing Agents. *Geophysical Research Letters*, *45*(21), 12,023–12,031. Retrieved 2019-07-15, from `https://agupubs.onlinelibrary.wiley.com/doi/abs/10.1029/2018GL079826` doi: 10.1029/2018GL079826

Stjern, C. W., Samset, B. H., Boucher, O., Iversen, T., Lamarque, J.-F., Myhre, G., … Takemura, T. (2020, November). How aerosols and greenhouse gases influence the diurnal temperature range. *Atmospheric Chemistry and Physics*, *20*(21), 13467–13480. Retrieved 2021-02-01, from `https://acp.copernicus.org/articles/20/13467/2020/` (Publisher: Copernicus GmbH) doi: https://doi.org/10.5194/acp-20-13467-2020

Swales, D. J., Pincus, R., & Bodas-Salcedo, A. (2018, January). The Cloud Feedback Model Intercomparison Project Observational Simulator Package: Version 2. *Geoscientific Model Development*, *11*(1), 77–81. Retrieved 2021-01-12, from `https://gmd.copernicus.org/articles/11/77/2018/` (Publisher: Copernicus GmbH) doi: https://doi.org/10.5194/gmd-11-77-2018

Zelinka, M. D., Klein, S. A., & Hartmann, D. L. (2012, June). Computing and Partitioning Cloud Feedbacks Using Cloud Property Histograms. Part II: Attribution to Changes in Cloud Amount, Altitude, and Optical Depth. *Journal of Climate*, *25*(11), 3736–3754. Retrieved 2020-04-28, from `https://journals.ametsoc.org/doi/full/10.1175/JCLI-D-11-00249.1` (Publisher: American Meteorological Society) doi: 10.1175/JCLI-D-11-00249.1

Zelinka, M. D., Klein, S. A., Taylor, K. E., Andrews, T., Webb, M. J., Gregory, J. M., & Forster, P. M. (2013, January). Contributions of Different Cloud Types to Feedbacks and Rapid Adjustments in CMIP5. *Journal of Climate*, *26*(14), 5007–5027. Retrieved 2019-07-15, from `https://journals.ametsoc.org/doi/full/10.1175/JCLI-D-12-00555.1` doi: 10.1175/JCLI-D-12-00555.1

Supporting Information for "Interpreting the Dependence of Cloud-Radiative Adjustment on Forcing Agent"

Contents of this file

Table S1. Experiment names and details for the experiments using common forcing agents in this paper. All experiments use the same control SSTs and sea ice.

Experiment name	Description
control	Pre-industrial climate (year 1850)
$10\times CH_4$	10 times concentrations of methane compared to pre-industrial levels
$2\times CO_2$	Doubling of CO_2 from pre-industrial level (284.7 ppm) to 569.4 ppm
10×BC	10 times concentrations of black carbon compared to pre-industrial levels
3%Sol	3% increase in the solar constant

Table S2. Experiment names and details for the simplified experiments used in this paper. All experiments use the same control SSTs and sea ice. The heating rates were prescribed as extra terms in the heating rate equations within CAM4's radiation scheme.

Experiment name	Description
atm_4	Homogeneous heating throughout the atmosphere for a horizontally homogeneous vertically-integrated forcing of 4 W m^{-2}
sfc_4	Homogeneous 4 W m^{-2} downwards flux at the surface
vloc_ϕhPa	Atmospheric heating defined through Eq. 1

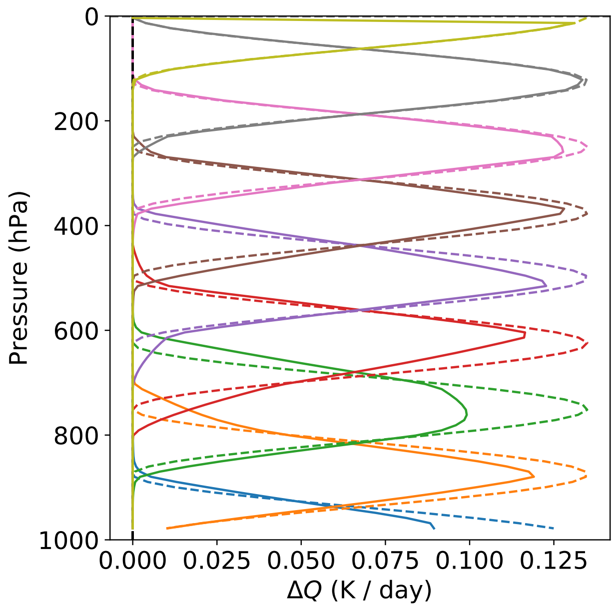

Figure S1. Heating profiles of all of the pulse heating experiments in this work. Dashed lines show the heating rates defined in Eq. 1 of the main text, whilst the solid lines show the profiles interpolated from the model grid.

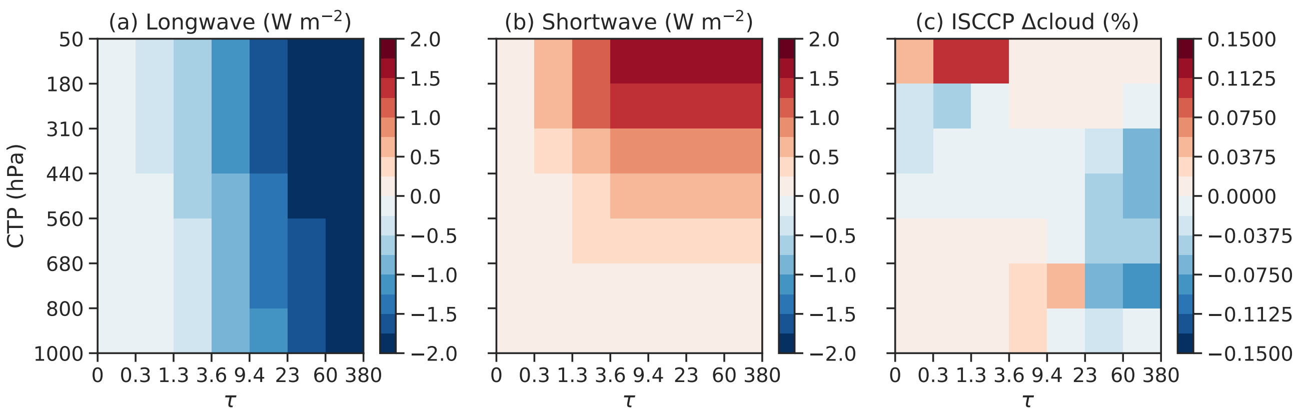

Figure S2. (a–b) Globally- (weighted by clear-sky surface albedo) and time-averaged histograms of the cloud kernels obtained from Zelinka et al. (2012). (c) Globally- and time-averaged histogram of the changes in satellite-observed cloud fraction between the 2×CO_2 and control cases.

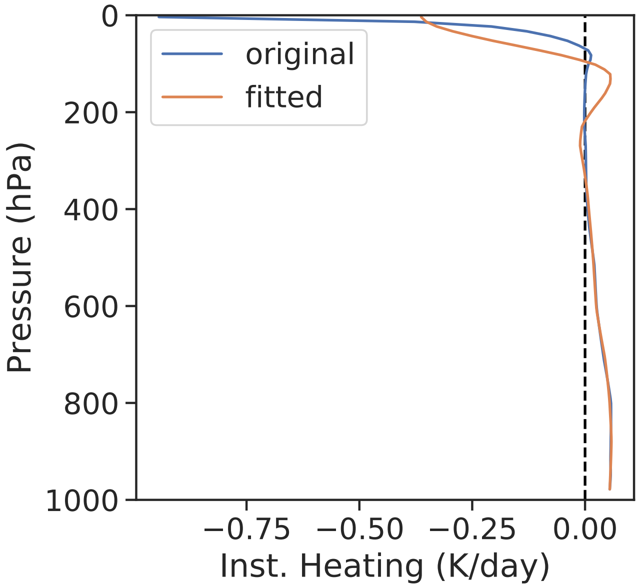

Figure S3. Heating profile for the $2\times CO_2$ experiment, with a linear fit of localised pulse heating experiments. The limited number of localised pulses results in issues with fitting to the stratospheric heating rates.

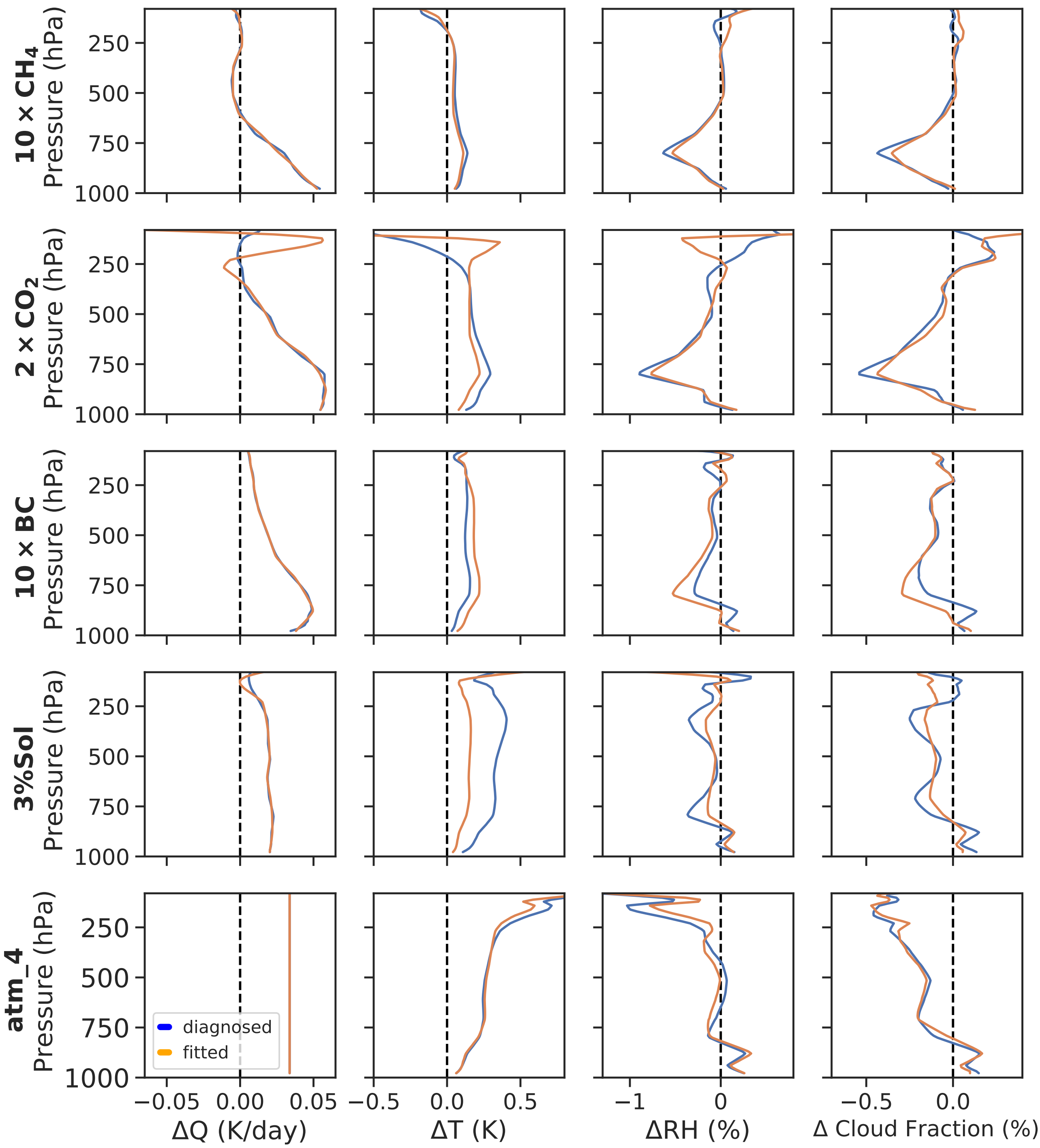

Figure S4. Global-mean vertical profiles of IRF (ΔQ) and rapid adjustments of temperature (ΔT), relative humidity (ΔRH) and cloud fraction. The same as Fig. 3 in the main text, except without contributions from surface forcings. Note that only the 3%Sol case changes significantly.